Catalysis Science & Technology

PAPER

View Article Online
View Journal | View Issue

Cite this: *Catal. Sci. Technol.*, 2014, **4**, 1644

Photocatalytic conversion of carbon dioxide into methanol in reverse fuel cells with tungsten oxide and layered double hydroxide photocatalysts for solar fuel generation†

Motoharu Morikawa,[a] Yuta Ogura,[b] Naveed Ahmed,[b] Shogo Kawamura,[b] Gaku Mikami,[b] Seiji Okamoto[b] and Yasuo Izumi*[b]

The phenomena of the photocatalytic oxidation of water and photocatalytic reduction of CO_2 were combined using reverse photofuel cells, in which the two photocatalysts, WO_3 and layered double hydroxide (LDH), were separated by a polymer electrolyte (PE) film. WO_3 was used for the photooxidation of water, whereas LDH, comprising Zn, Cu, and Ga, was used for the photoreduction of CO_2. For this process, photocatalysts pressed on both sides of the PE film were irradiated with UV-visible light through quartz windows and through the space in carbon electrode plates and water-repellent carbon paper for both gas flow and light transmission. 45% of the photocatalyst area was irradiated through the windows. The protons and electrons, which were formed on WO_3 under the flow of helium and moisture, transferred to the LDH *via* the PE and external circuit, respectively. Methanol was the major product from the LDH under the flow of CO_2 and helium. The observed photoreduction rates of CO_2 to methanol accounted for 68%–100% of photocurrents. This supports the effectiveness of the combined photooxidation and photoreduction mechanism as a viable strategy to selectively produce methanol. In addition, we tested reverse photofuel cell-2, which consisted of a WO_3 film pressed on C paper and LDH film pressed on Cu foil. The photoelectrodes were immersed in acidic solutions of pH 4, with the PE film distinguishing the two compartments. Both the photoelectrodes were completely irradiated by UV-visible light through the quartz windows. Consequently, the photocurrent from the LDH under CO_2 flow to WO_3 under N_2 flow was increased by 2.4–3.4 times in comparison to photofuel cell-1 tested under similar conditions. However, the major product from the LDH was H_2 rather than methanol using photofuel cell-2. The photogenerated electrons in the irradiated area of the photocatalysts were obliged to diffuse laterally to the unirradiated area of photocatalysts in contact with the C papers in photofuel cell-1. This lateral diffusion reduced the photocatalytic conversion rates of CO_2, despite the advantages of photofuel cell-1 in terms of selective formation and easy separation of gas-phase methanol.

Received 23rd November 2013,
Accepted 18th February 2014

DOI: 10.1039/c3cy00959a

www.rsc.org/catalysis

Introduction

The photocatalytic conversion of CO_2 into fuels has emerged as an attractive option,[1] in terms of both reducing the increased concentration of atmospheric CO_2 as well as generating renewable hydrocarbon fuels that can directly be supplied to our present energy infrastructure. Analogous to photosynthesis, the photocatalytic conversion of CO_2 involves (1) the photooxidation of water and (2) the photoreduction of CO_2 corresponding to photosystem II, and subsequent dark reactions to incorporate CO_2 into carbohydrates utilizing NADPH formed in photosystem I.[2,3]

Thus far, several researchers have reported photocatalytic cells for water oxidation[2] and proton reduction[4–6] by using Pt–WO_3 and Pt–$SrTiO_3$,[7] as well as TiO_2 and Pt–TiO_2 separated by a polymer electrolyte (PE) film.[8] The combination of steps 1 and 2 of the photocatalytic conversion of CO_2 has been realized using metal complexes and enzymatic photocatalysts.[9] To the best of our knowledge, there are no studies reporting on the combination of semiconductor photocatalysts for the photocatalytic conversion of CO_2. In principle, the combination of steps 1 and 2 can be regarded as *reverse* fuel cell operation. This process is considered to be a *reverse* mechanism because the products generated by

[a] *Department of Nanomaterial Science, Graduate School of Advanced Integration Science, Chiba University, Yayoi 1-33, Inage-ku, Chiba 263-8522, Japan*
[b] *Department of Chemistry, Graduate School of Science, Chiba University, Yayoi 1-33, Inage-ku, Chiba 263-8522, Japan. E-mail: yizumi@faculty.chiba-u.jp*
† Electronic supplementary information (ESI) available. See DOI: 10.1039/c3cy00959a

conventional fuel cells, *i.e.*, CO_2 and H_2O, react to form methanol and O_2, which are the reactants in the conventional fuel cell. In fact, the original concept of reaction between CO_2 and H_2O was proposed[10–12] and demonstrated to be a reverse fuel cell operation,[13] rather than a photocatalytic conversion process.

In this paper, we report the fabrication of a polymer electrolyte fuel cell (PEFC; Fig. 1) comprising tungsten oxide (WO_3) and layered double hydroxide (LDH) photocatalysts, and a photofuel cell consisting of acid solutions separated by a PE film (Fig. 2). In addition, we experimentally demonstrate solar fuel generation,[10,14–17] in which the photooxidation of water results in the transfer of protons and electrons to form fuel combined with CO_2.

The primary advantage of using photofuel cells is the band potential of two photocatalysts, which is tunable in comparison with the oxidation and reduction potential of independent reactions, by the choice of the elemental composition of the semiconductor catalysts. Traditionally, WO_3 has been the catalyst of choice for the photooxidation of water (E° = 1.23 − 0.0591 × pH V, 298 K), primarily because of the relatively positive band potential.[18] Similarly, LDH is an unusual class of layered materials comprising positively charged cation layer and interlayer anionic species such as CO_3^{2-}.[19] Recently, researchers have demonstrated the photocatalytic conversion of CO_2 into CO and methanol in water[20] or hydrogen[21–23] by using LDHs comprising Ni, In, Zn, Cu, and Ga. From these reports, we chose LDH compounds comprising Zn, Cu, and Ga for the photoreduction of CO_2 in this study.

In addition, the added advantage of using a photofuel cell is that the photocatalysts used are earth-abundant elements and are relatively inexpensive. Furthermore, the products formed as a result of photocatalysis can be readily separated in the gas phase. This is a unique advantage of using a photofuel cell based on PEFC (Fig. 1), as reported for the electrocatalytic cell separated by Nafion.[24]

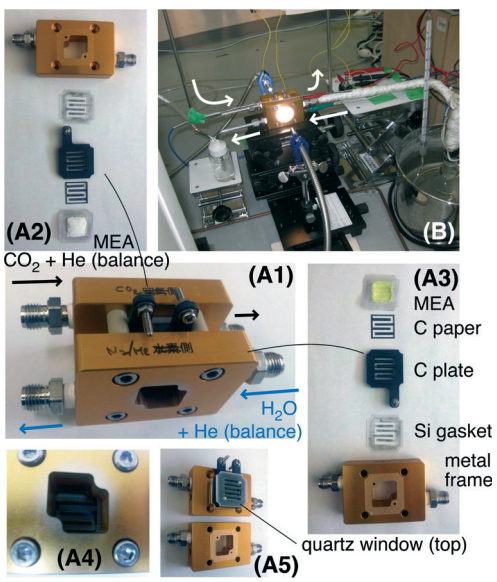

Fig. 1 Fabricated photofuel cell-1. The figures show the different components (A) and a photocatalytic test with flowing moisture + He (balance) (front side) and circulating CO_2 + He (balance) (rear side) (B). A1 depicts photofuel cell-1 at the center of B. A2 and A3 depict components of the photocathode and photoanode, respectively. A4 is a view of the window of photofuel cell-1. A5 depicts the assembled quartz window, silicon gasket, C electrode plate, C paper, silicon gasket, and WO_3–Nafion–LDH1 assembly.

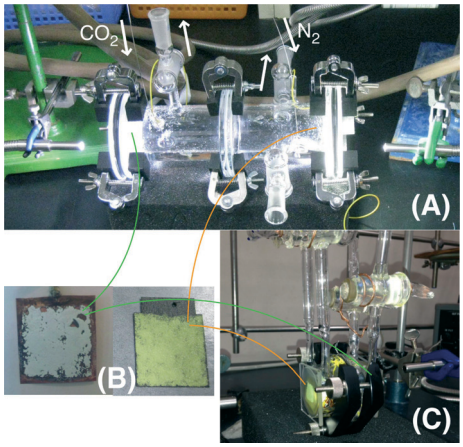

Fig. 2 Fabricated photofuel cell-2. The figures show the different components (A) and LDH1 mounted onto Cu foil and WO_3 mounted onto water-repellent C paper (B, left to right). The smaller cell-2 was also used in which the LDH1 side (right) was circulated with CO_2 gas (C).

Experimental

Synthesis of WO_3 and LDH consisting of Zn, Cu, and Ga

WO_3 was synthesized by the calcination of ammonium paratungstate pentahydrate $(NH_4)_{10}^{+}(W_{12}O_{41})^{10-}\cdot 5H_2O$ (Aldrich, >99.99%) in air at 973 K for 4 h.

Nitrogen adsorption isotherm measurements were performed at 77 K within the pressure range 1.0–90 kPa in a vacuum system connected to diffusion and rotary pumps (10^{-6} Pa) and equipped with a capacitance manometer (Models CCMT-1000A and GM2001, ULVAC). The Brunauer–Emmett–Teller surface area (SA) was calculated on the basis of eight-point measurements between 10 and 46 kPa (P/P_0 = 0.10–0.45) on the adsorption isotherm. The samples were evacuated at 383 K for 2 h before the measurements. The specific SA of WO_3 thus obtained was estimated to be 20 $m^2\ g^{-1}$.

In this study, we synthesized LDH1 $[Zn_{1.5}Cu_{1.5}Ga(OH)_8]_2^{+}$ $[Cu(OH)_4]^{2-}\cdot mH_2O$ starting from nitrates of Zn, Cu, and Ga and ammonium tetracholorocupurate dihydrate at pH 8. Details of the experimental procedure adopted for the synthesis of LDH1 have been reported in the literature.[22,23] The exact molecular formula of LDH1, as determined by using extended X-ray absorption fine structure analysis, was found to be $Zn_3Cu_3Ga_2(OH)_{13}[(\mu\text{-}O)_3Cu(OH)(H_2O)_2]\cdot mH_2O$, with the dehydration of three water molecules.[21] Furthermore, the specific SA of LDH1 was estimated to be 62 $m^2\ g^{-1}$.

Design of photofuel cell-1

For this process, 95 mg of WO_3 or 45 mg of LDH1 was suspended in 5% of Nafion dispersion solution (DE521, Wako Pure Chemical; 0.2 mL) and 1-propanol (0.1 mL) and

separately mounted onto water-repellent carbon paper (C paper, TGP-H-060H, Chemix) in an area of 4 cm^2. Subsequently, WO_3 mounted onto the C paper was pressed with LDH1 mounted onto the C paper and separated using a PE film (Nafion, NR-212, Dupont) of thickness 50 μm. The layers were pressed using a tabletop press (Model SA-302, Tester Sangyo Co.) by applying a pressure of 2.0 MPa at 393 K for 10 min. Then the C papers on both sides were carefully removed, resulting in the formation of the WO_3–Nafion–LDH1 assembly.

The electronic conductivity of WO_3 and LDH1 was improved by mixing WO_3 (95 mg) and LDH1 (45 mg) with a minimum amount of C black (0.2 mg; Vulcan XC72, specific SA 250 $m^2\ g^{-1}$) using a mortar and pestle. Subsequently, the obtained WO_3 and LDH1 were pressed together with a Nafion film separator to form a WO_3/C–Nafion–LDH1/C assembly, by using a procedure similar to that adopted for the fabrication of WO_3–Nafion–LDH1.

Photofuel cell-1 designed in this study is shown in Fig. S1 (ESI†). The prepared WO_3–Nafion–LDH1 assembly was first sandwiched by a water-repellent C paper and then by C electrode plates, both *via* a serpentine route (the space section for gas flow and window for light; Fig. 1A2, A3). Subsequently, this assembly was sandwiched by quartz window plates. It should be noted that the C paper and C plate were fixed in an area of 2.2 cm^2 and the area of the serpentine route was 1.8 cm^2 out of the total 4 cm^2 of each quartz window (Fig. 1). Therefore, among a catalyst area of 4 cm^2, the area of 1.8 cm^2 (45%) was irradiated through the serpentine route whereas the area of 2.2 cm^2 (55%) was blocked by the C paper and C plate from light (Fig. S1†).

Photofuel cell-1 offers the advantage of easy separation of gas-phase products, including methanol. However, a disadvantage associated with the design of the photofuel cell is that only 45% of the photocatalysts get irradiated.

CO_2 conversion tests using photofuel cell-1

The fabricated photofuel cell-1 was further tested for its CO_2 conversion efficiency. As the first step, all solvents included in the Nafion dispersion solution were removed by flowing N_2 gas at a rate of 100 mL min^{-1} through a water bubbler maintained at 343 K, independently to WO_3 and LDH1 for 10 h. Subsequently, WO_3 in the system was purged with He gas at a rate of 50 mL min^{-1} through the water bubbler at 323 K. CO_2 (3.5%) with the remaining He gas (total 101 kPa) was circulated in a glass line at a rate of 450 mL min^{-1} through LDH1 (Fig. 1A1).

WO_3 and LDH1 on the Nafion film were irradiated by UV-visible light from a 500 W xenon arc lamp (Ushio, Model SX-UID502XAM) *via* a two-way quartz fiber light guide of 1 m (San-ei Electric Co., Model 5Φ-2B-1000 L) for 10 h (Fig. 1B). The distance between fiber light exit and photofuel cell window was maintained at 50 mm. The light intensity on the photocatalyst was 33 mW cm^{-2}. With the onset of irradiation, the photocatalyst temperature reached as high as 315 K.

The gas circulating through LDH1 was analyzed by an inline gas chromatograph equipped with a thermal conductivity detector (GC-TCD; Shimadzu, Model GC-8A), using He as the carrier gas. The columns were packed with Molecular Sieve 13X-S and polyethylene glycol-6000 supported on Flusin P (GL Science). The current between the two electrodes (Fig. 1A, B) was monitored simultaneously.

Design of photofuel cell-2

We also designed photofuel cell-2, as shown in Fig. 2. Both photofuel cells were compared for their performance.

For the fabrication of photofuel cell-2, 95 mg of WO_3 was suspended in 5% of Nafion dispersion solution (0.24 mL) and 1-propanol (0.16 mL) and mounted onto water-repellent C paper in an area of 4 cm^2. WO_3 mounted onto the C paper was then covered with a Kapton film (200H, Dupont) of thickness 50 μm and pressed using a tabletop press (SA-302) by applying a pressure of 2.0 MPa at 393 K for 10 min. Then, the Kapton film was carefully removed to obtain the WO_3/C photoelectrode (Fig. 2B, right). In a separate process, 45 mg of LDH1 was suspended in 5% of Nafion dispersion solution (0.24 mL) and 1-propanol (0.16 mL) and mounted onto Cu foil (2.3 × 2.5 cm^2) of thickness 30 μm in an area of 4 cm^2. LDH1 mounted onto the Cu foil was then covered with a water-repellent C paper and pressed using a tabletop press (SA-302) by applying a pressure of 2.0 MPa at 393 K for 10 min. Following that, the C paper was carefully removed to obtain the LDH1/Cu photoelectrode. In addition, the LDH1/Cu photoelectrode was prepared by dispersing LDH1 in 1-propanol (0.4 mL) instead of Nafion dispersion solution in a manner similar to that for LDH1/Cu. LDH1 is sticky and attached to Cu foil even in the absence of Nafion (Fig. 2B, left).

CO_2 conversion tests using photofuel cell-2

As the next step, we analyzed the CO_2 conversion performance of photofuel cell-2. For this, the prepared WO_3/C and LDH1/Cu photoelectrodes were immersed in aqueous hydrochloric acid solution (50 mL at each electrode) at pH 4.0, separated by a 50 μm-thick Nafion film at the center of the cell (Fig. 2A). Subsequently, N_2 and CO_2 were bubbled at a rate of 50 mL min^{-1} through the sides of WO_3 and LDH1, respectively. Both photocatalysts were irradiated using a 500 W Xe arc lamp *via* a two-way quartz fiber light guide. The photocatalysts were irradiated from both sides (Fig. 2A) for 30 min and kept in the dark for 30 min. The light on/off cycle was repeated five times. The distance between the fiber light exit and the photoelectrode was maintained at 50 mm. The light intensity on the photocatalyst at this position was 33 mW cm^{-2}.

Moreover, a smaller photofuel cell-2 was also fabricated (Fig. 2C) to make the product concentration relatively higher for the GC analysis. 15 mL of HCl solution was introduced at each electrode. CO_2 was circulated in a glass line at a rate of 450 mL min^{-1} through the side of LDH1. The other conditions were similar to that for Fig. 2A. The gas circulated through LDH1 was analyzed by the inline GC-TCD (Model GC-9A) using

Ar as the carrier gas and also a GC-flame ionization detector (FID; Shimadzu, Model GC-18A) equipped with a capillary column Ultra ALLOY-5 (Frontier Laboratories; inner diameter 250 μm, length 30 m) using He as the carrier gas.

Results

CO_2 to methanol conversion in photofuel cell-1

WO_3 on one side of the Nafion film was irradiated with UV-visible light under the flow of He and moisture, while LDH1 on the other side of the Nafion film was irradiated with UV-visible light under the flow of CO_2 (3.5%) (Fig. 1B). The main product of the reaction was methanol, whose amount monotonously increased as a function of time irradiated under light (Fig. 3, entry a). Other gases generated during the reaction, including CO and methane, were not detected, probably because the amount was below the detection limit of GC. Similarly, H_2 generation could not be monitored, as He was the carrier gas. In this process, the methanol formation rate was estimated to be 0.045 μmol h^{-1} g_{cat}^{-1}, considering that the LDH1 photoelectrode was irradiated through the serpentine route and the effective illumination area is 45% (Fig. 1A4).

During the total illumination period of 10 h, the current from the LDH1 electrode to the WO_3 electrode was stabilized to a constant value of 0.22 μA in 1.6 h (Fig. 4a). The current corresponds to an electron flow rate of 0.40 μmol-e^- h^{-1} g_{LDH}^{-1} from WO_3 to LDH1 (Table 1a). Here, 68% of the photocurrent was accounted for by the six-electron reduction reaction (6 × 0.045 μmol-CH_3OH h^{-1} g_{cat}^{-1} = 0.27 μmol-e^- h^{-1} g_{cat}^{-1}) from CO_2 to methanol.

Furthermore, we analyzed the effects of mixing C black with the photoelectrodes by comparing the CO_2 conversion performance of the WO_3/C–Nafion–LDH1/C assembly with that of the WO_3–Nafion–LDH1 described above. The CO_2 conversion results of the WO_3/C–Nafion–LDH1/C assembly in the photofuel cell are plotted in Fig. 3, entry b. As seen from the figure, the methanol formation rate is 0.029 μmol h^{-1} g_{cat}^{-1}. This indicates a reduction in the methanol formation rate by 36% with the addition of C black to LDH1 and WO_3. The lower formation rate should be due to lower light

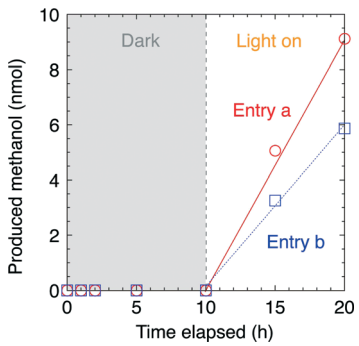

Fig. 3 Time evolution of the formation of methanol in photofuel cell-1 consisting of WO_3 and LDH1 (a) and WO_3 and LDH1 mixed with C black (b). The photocatalysts were in the dark for 10 h and UV-visible light was irradiated in the next 10 h (a, b).

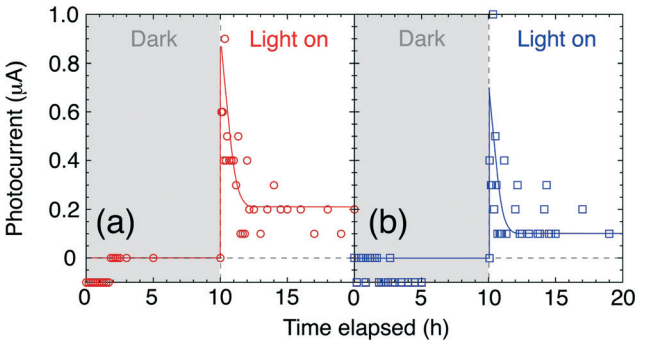

Fig. 4 Time evolution of the photocurrent generated during CO_2 conversion tests using photofuel cell-1 consisting of WO_3 and LDH1 (a) and WO_3 and LDH1 both mixed with C black (b). The photocatalysts were in the dark for 10 h and UV-visible light was irradiated in the next 10 h (a, b).

penetration depth into both photocatalyst layers mixed with C rather than the effect of improved electron conductivity by mixing the photocatalysts with C. During the test, the photocurrent from the LDH electrode to the WO_3 electrode stabilized to a constant value of 0.10 μA in 1.6 h (Fig. 4b). The constant current corresponds to an electron flow rate of 0.18 μmol-e^- h^{-1} g_{LDH}^{-1} from WO_3/C to LDH1/C (Table 1b). Most of the current was accounted for by the six-electron reduction reaction (6 × 0.029 μmol-CH_3OH h^{-1} g_{cat}^{-1} = 0.17 μmol h^{-1} g_{cat}^{-1}) from CO_2 to methanol.

The generated photocurrents decreased in the initial 1.6 h of irradiation both in Fig. 4a and b. In comparison to the rather constant formation of methanol (Fig. 3), a major part of the initial photocurrents may not be due to photocatalysis.

In this study, we performed two blank tests. One blank test was performed at 323 K, which is higher than the maximum temperature (315 K) of kinetic tests irradiated by light, under dark conditions and flow of He and moisture to WO_3 and flow of CO_2 (3.5%) and the remaining He to LDH1. The other blank test was performed with light irradiation under the flow of He and moisture to WO_3, and the flow of He to LDH1. For both tests, we could not detect products above the detection limit of GC. The photocurrent was negligible after 2 h of reaction.

CO_2 to methanol conversion using photofuel cell-2

The CO_2 photoconversion performance of photofuel cell-1 was compared with that of photofuel cell-2 containing WO_3 and LDH1 immersed in acid solutions, and fully exposed to light.

For the photofuel cell containing 95 mg of WO_3 and 45 mg of LDH1 separately mounted onto C paper and Cu foil, respectively (Fig. 2A, B), the photocurrent gradually increased within 15–20 min of irradiation under UV-visible light and gradually decreased to background levels within 10–15 min in the dark (Fig. 5a).

The maximum photocurrent from the LDH1 electrode to the WO_3 electrode was 1.15 μA, as determined from five on/off cycles of light irradiation. The photocurrent corresponded

Table 1 Comparison of photocurrents generated during the CO_2 conversion tests using the photofuel cells designed in this study

Entry	Cell type	WO_3[a] support	LDH1[b] support	Current (μA)	e^- flow rate (μmol h^{-1} $g_{LDH}{}^{-1}$)	MeOH or H_2 form rate (μmol h^{-1} $g_{LDH}{}^{-1}$)
a	Photofuel cell-1	Nafion film	Nafion film	0.22	0.40[d]	0.045 (MeOH)[d]
b		Nafion film (C black mixed[c])	Nafion film (C black mixed[c])	0.10	0.18[d]	0.029 (MeOH)[d]
c	Photofuel cell-2	C paper	Cu foil	1.15	0.96	0.49 (H_2)
d		C paper	Cu foil (no Nafion disp sol used[e])	1.63	1.36	0.67 (H_2)

[a] 95 mg. [b] 45 mg. [c] 0.2 mg. [d] Divided by exposed LDH1 sample to light (45 mg × 0.45). [e] LDH1 was dispersed in 1-propanol only and mounted on Cu foil.

to an electron flow rate of 0.96 μmol h^{-1} $g_{LDH}{}^{-1}$, a factor of 2.4 times greater than that using photofuel cell-1 (Table 1c, a). In this comparison, the electron flow rates were estimated by the area of photocatalyst exposed to light irradiation, *e.g.*, 45% and 100% for photofuel cell-1 and photofuel cell-2, respectively.

In addition, we performed the CO_2 photoconversion test using photofuel cell-2 consisting of WO_3 (95 mg) on C paper and LDH1 (45 mg) on Cu foil, which was prepared without the Nafion dispersion solution. The change in photocurrent during the five on/off cycles of light is depicted in Fig. 5b. As seen from the figure, the photocurrent increases gradually under light and decreases gradually to background level in the dark. This trend is very similar to that shown in Fig. 5a. However, the maximum photocurrent (1.63 μA) was found to increase by a factor of 1.42 times with the elimination of Nafion in the LDH1 photoelectrode mounted on Cu foil. The photocurrent corresponded to an electron flow rate of 1.36 μmol h^{-1} $g_{LDH}{}^{-1}$, which was 3.4 times greater than that using photofuel cell-1 (Table 1d, a).

Both the gas circulated through LDH1 and the acid solution for LDH1 were analyzed in a separate test using a smaller photofuel cell-2 (Fig. 2C). The time evolution is depicted in Fig. 6. When WO_3 on C paper was purged with N_2 gas and LDH1 on Cu foil was circulated with CO_2, both prepared using a Nafion dispersion solution, hydrogen was a major product from LDH1 (Fig. 6, entry a) at a formation rate of 0.49 μmol-H_2 h^{-1} $g_{LDH}{}^{-1}$. H_2 formation was also observed in dark cycles. This fact is related to the slow decrease of photocurrent in dark cycles (Fig. 5a), suggesting diffusion control. Most of the current (0.96 μmol-e^- h^{-1} $g_{LDH}{}^{-1}$) was accounted for by the two-electron reduction reaction (2 × 0.49 μmol-H_2 h^{-1} $g_{LDH}{}^{-1}$ = 0.98 μmol h^{-1} $g_{LDH}{}^{-1}$; Table 1c).

When WO_3 on C paper was purged with N_2 gas and LDH1 on Cu foil was circulated with CO_2, prepared without the Nafion dispersion solution, the hydrogen formation under UV-visible light irradiation became faster, at a rate of 0.67 μmol-H_2 h^{-1} $g_{LDH}{}^{-1}$ (Fig. 6b). Most of the current (1.36 μmol-e^- h^{-1} $g_{LDH}{}^{-1}$; Fig. 5b) was accounted for by the two-electron reduction reaction (2 × 0.67 μmol-H_2 h^{-1} $g_{LDH}{}^{-1}$ = 1.34 μmol h^{-1} $g_{LDH}{}^{-1}$; Table 1d).

In both tests in Fig. 6a and b, other gases generated during the reaction through LDH1 were not detected above the detection limit of GC-TCD. The acid solution for LDH1 in photofuel cell-2 under the conditions of Fig. 6b (Fig. 2C) irradiated under UV-visible light for 10 h was analyzed by GC-FID, but methanol was not detected above the detection limit (4.83 pmol in 1.0 μL injection). The detection limit corresponded to the formation rate of 0.16 μmol-CH_3OH h^{-1} $g_{LDH}{}^{-1}$. Taking the six-electron reduction into account, the detection limit was 0.96 μmol-e^- h^{-1} $g_{LDH}{}^{-1}$ *versus* the observed current of 1.36 μmol-e^- h^{-1} $g_{LDH}{}^{-1}$ (Fig. 5b). Therefore methanol was not the major product in photofuel cell-2.

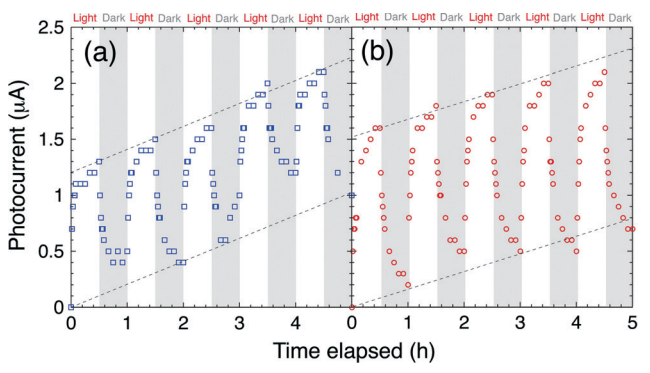

Fig. 5 Time evolution of photocurrent generated during CO_2 conversion tests using photofuel cell-2 comprising WO_3 on C paper, prepared using Nafion suspension solution (a, b) and LDH1 on Cu foil, prepared using Nafion suspension solution (a) and prepared using 1-propanol without Nafion (b).

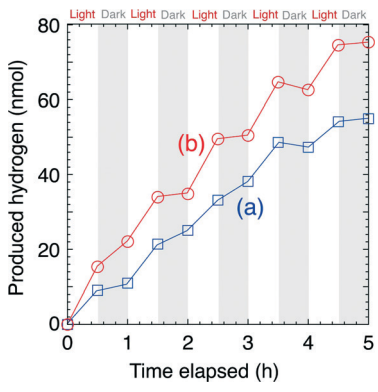

Fig. 6 Time evolution of the formation of hydrogen during CO_2 conversion tests using photofuel cell-2 comprising WO_3 on C paper, prepared using Nafion dispersion solution (a, b) and LDH1 on Cu foil, prepared using Nafion suspension solution (a) and prepared using 1-propanol without Nafion (b).

Discussion

It is well known that the mechanism underlying the photocatalytic splitting of water using WO_3 under UV irradiation is *via* the following equation.[25,26]

$$2H_2O \rightarrow O_2 + 4H^+ + 4e^- \quad (1)$$

In this study, WO_3 exhibited constant oxygen generation upon irradiation by UV-visible light in the presence of a sacrificial oxidant (Ag^+).[27] The potentials for the photoreduction reactions, *e.g.*, H_2 formation, are beyond the bandgap energy of WO_3.[18] Thus, the protons generated in this process transferred to LDH1 *via* Nafion film in the case of photofuel cell-1, and *via* the acid solution and Nafion film in the case of photofuel cell-2. On the other hand, the electrons generated in this process transferred to LDH1 *via* the external circuit (Scheme 1).

On comparing the photocurrent generated in photofuel cell-1 and photofuel cell-2 with the same types and amounts of photocatalysts, it was observed that photofuel cell-2 generated a higher photocurrent. This suggests that proton diffusion in the HCl solutions (pH 4) of photofuel cell-2 (Table 1c, d) is sufficiently high and that the diffusion of protons in 50 μm-thick Nafion film is relatively critical. The conductivity of Nafion film at a relative humidity of 10–100% was reported to be 79 mS cm^{-1} based on electrochemical impedance spectroscopy.[28] If the applied voltage was assumed to be 1 V, the conductivity corresponded to proton conductivity of the order of 10^{-5} mol h^{-1} for Nafion film of thickness 50 μm. In contrast, the proton diffusion rate in acid solution (pH) can be estimated based on the catalytic rate of the diffusion-limited reaction.[29] The hydrogen formation rate from an $Fe_2S_2(CO)_4[P(OCH_3)_3]_2$ complex was of the order of 10^{-1} mol h^{-1}. Apparently, proton conduction in Nafion film is more critical compared to that in acid solution, but it is somewhat faster compared to the charge flow in the cells of this study (3.6–61 nmol h^{-1}; Table 1), suggesting rate control primarily by surface reactions.

Fig. 5a and b show a gradual increase in the background current. This could primarily be attributed to the slow supply of protons to LDH1, leading to a concentration gradient of solutions between the WO_3 side and LDH1 side. Alternatively, the pH of the solution in the LDH1 side would have increased with the increase in temperature from 290 to 310 K due to the solubility dependence of CO_2 during the five on/off irradiation cycles. Consequently, to compensate the pH change, the background current might have increased gradually.

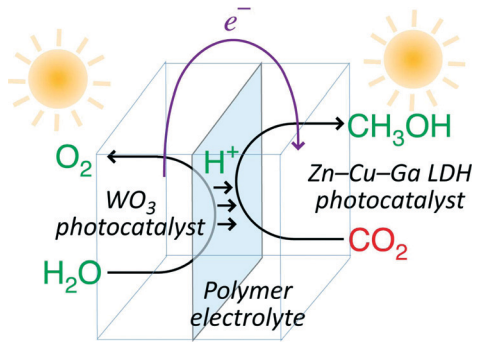

Scheme 1 Schematic illustration of the flow of materials and electrons during photocatalytic CO_2 conversion in reverse photofuel cell-1 consisting of WO_3 and LDH1.

Reaction (1) in the presence of the WO_3 catalyst is followed by reaction (2) over LDH1.

$$CO_2 + 6H^+ + 6e^- \rightarrow CH_3OH + H_2O \quad (2)$$

The mechanism underlying reaction (2) seems to be similar to that of reaction (2′), which has been reported for LDH1 and $[Zn_{1.5}Cu_{1.5}Ga(OH)_8]_2^+CO_3^{2-}\cdot mH_2O$ photocatalysts.[21–23] More specifically, the importance of protonation to the one-electron-reduced CO_2 species has been discussed while explaining the formation of formic acid[30] and methane[31] in the presence of TiO_2 and Zn–Ge oxynitride.[32] Specific reaction pathways have been proposed for reaction (2) or reaction (2′), which result in methanol (or CO/methane) *via* the formation of formaldehyde,[21,23,33] carbene,[33] and glyoxal[33] by multiple protonation steps and electron supply.

$$CO_2 + 3H_2 \rightarrow CH_3OH + H_2O \quad (2')$$

Similar to the reports for reaction (2′),[21–23] methanol was the major product formed in photofuel cell-1. 68%–100% of electron production/consumption during the steady-state period, between 2 and 10 h, in photofuel cell-1 (Fig. 3 and 4) can be attributed to the conversion of CO_2 to methanol. We evaluated the photocatalytic performance starting from H_2O and CO_2 according to the photocurrent from LDH1 to WO_3 electrodes in the photofuel cells (Table 1).

The excessive photocurrents observed in the initial 1.6 h in photofuel cell-1 corresponded to 0.022 μmol of electrons (Fig. 4a, b). A major part of the initial photocurrents are not due to photocatalysis. One of the possibilities is that WO_3 proceeded reaction (1) whereas the supplied electrons from WO_3 to the photocathode were consumed non-catalytically, *e.g.* the partial reduction of Cu^{II} sites in LDH1 under irradiation. In this study, the amount of Cu used in the cell was 180 μmol. We tried to detect reduced Cu^{I} sites among major Cu^{II} sites in LDH1 used for the tests in Fig. 5b & 6b by synchrotron Cu K-edge X-ray absorption spectroscopy at KEK-PF & SPring-8.[21,23,34] However, 120 ppm of Cu^{I} at maximum was hard to detect experimentally.

The major generation of hydrogen from the photocathode (LDH1) was directly monitored in photofuel cell-2 (Fig. 6). In contrast, the part of the photocurrent that was not attributed to the conversion of CO_2 to methanol, which is less than 32% of total photocurrents (Table 1), may be ascribed to the formation of hydrogen in photofuel cell-1. The reduction potential for reaction (2) ($E^\circ = -0.32 - 0.0591 \times$ pH V), in which methanol concentration is negligible compared to proton concentration, is similar to that for reaction (3) ($E^\circ = 0 - 0.0591 \times$ pH V).[35] In the blank test with light irradiation

under the flow of He and moisture to WO_3, and He to LDH1 in photofuel cell-1, the photocurrent was negligible, after 2 h of reaction. Thus, H_2 formation was negligible but further photocatalytic reduction to methanol should proceed at the interface of LDH1 and the gas (CO_2 & He) in photofuel cell-1 whereas reaction (3) predominantly proceeded at the interface of LDH1 and the acid solution of pH 4.0 in photofuel cell-2. The observed clear contrast in selectivity is due to gaseous CO_2 (3.5%) in photofuel cell-1 (methanol formation) *versus* the limited solubility of CO_2 in water in photofuel cell-2 (hydrogen formation).

$$2H^+ + 2e^- \rightarrow H_2 \quad (3)$$

In summary, efficient CO_2 conversion to methanol can be observed over LDH1 in photofuel cell-1, which is analogous to the CO_2 photoconversion to methanol in CO_2 + H_2 mixed gases,[21–23] whereas hydrogen was preferably formed in photofuel cell-2.

Although the major photocatalytic products (methanol or H_2) were different, the electron flow rates in photofuel cell-2 (0.96–1.36 μmol h^{-1} $g_{LDH}{}^{-1}$; Table 1c, d) were observed to be significantly higher, by 2.4–3.4 times, when compared to those in photofuel cell-1 (0.40 μmol h^{-1} $g_{LDH}{}^{-1}$; Table 1a). A reason for this is the longer electron diffusion path from the WO_3 layer to the C electrode and that from the C electrode to the LDH1 layer for photofuel cell-1. In particular, the proton transfer in the serpentine area (Fig. 1A2–5) should be good, while the electrons separated from holes in the irradiated serpentine area of photocatalysts must laterally diffuse to the unirradiated area of photocatalysts, C paper, and then to the C electrode (anode) connected to the external circuit. For the photocathode, the electron flow from the C paper to the unirradiated area of LDH1 and then laterally to the irradiated serpentine area of LDH1 is needed. For photofuel cell-2, the electrons separated under irradiation easily diffuse into the thin WO_3 photocatalyst vertically to the C paper,[36] and from the C paper vertically to the thin LDH1 (Fig. 2A, C).

Of the two photofuel cells analyzed in this study, the maximum photocurrent was observed (Fig. 5b) in photofuel cell-2 consisting of WO_3 and the LDH1 photoelectrode on Cu foil prepared without Nafion dispersion solution (Fig. 2B). The current was quantitatively in accord with dominant H_2 formation (Fig. 6b). Nafion dispersion solution used to mount LDH1 on Cu foil had a negative effect in covering the active photoreduction sites (Table 1c, d). Furthermore, X-ray diffraction studies of the LDH1 sample indicate that the layered structure of LDH1 is not destroyed during the photoreduction test for 5 h. In spite of this, LDHs as hydroxide-based materials needing to be in close contact with Nafion dispersion solution/film would be unstable in the longer-term application of photofuel cell-1.

Conclusions and future prospects

A reverse photofuel cell to form O_2 and methanol was designed using WO_3 as the photooxidation catalyst of water and a LDH, $Zn_3Cu_3Ga_2(OH)_{13}[(\mu\text{-}O)_3Cu(OH)(H_2O)_2]\cdot mH_2O$, as the photoreduction catalyst of CO_2. This cell could be used to enable solar fuel generation if optimum photooxidation/reduction catalysts are chosen independently.

Photofuel cell-1, which was designed on the basis of PEFC, was advantageous in terms of the easy separation of methanol gas as the major product. On the other hand, solar fuel generation was limited, especially from the photoelectron flow efficiency viewpoint. The electrons generated in WO_3 by the photooxidation of water were obliged to move laterally to the unirradiated area of WO_3 and then to carbon, and from carbon to the unirradiated area of LDH1 and then laterally to the irradiated area of LDH1.

Photofuel cell-2, consisting of independent photoelectrodes immersed in acid solution (pH 4), had higher photocurrents, by 2.4–3.4 times. However, the reaction on LDH1 caused H_2 formation and methanol was not found above the detection limit of GC-FID. Future studies are required to improve photofuel cell-1 and to control the potential of the harder step, *i.e.*, CO_2 photoreduction at the photocathode by using sustainable sources such as solar cells.[27]

Acknowledgements

The authors are grateful for the financial support from the Grant-in-Aid for Scientific Research C (proposal no. 22550117) from Monbukagakusho and the Feasibility Study Stage of A-STEP (proposal no. AS231Z01459C and AS251Z00906L) from the Japan Science and Technology Agency. The X-ray absorption experiments were performed with the approvals of the Photon Factory Proposal Review Committee (no. 2011G033 and 2009G552) and the grant of the Priority Program for Disaster-Affected Quantum Beam Facilities (2011A1977, SPring-8 & KEK).

Notes and references

1 M. Mikkelsen, M. Jørgensen and F. C. Krebs, *Energy Environ. Sci.*, 2010, **3**, 43.
2 J. H. Alstrum-Acevedo, M. K. Brennaman and T. J. Meyer, *Inorg. Chem.*, 2005, **44**, 6802.
3 D. Voet and J. G. Voet, *Biochemistry*, Wiley, New York, 2nd edn, 1995, ch. 22, pp. 626–661.
4 K. S. Joya, Y. F. Joya, K. Ocakoglu and R. van de Krol, *Angew. Chem., Int. Ed.*, 2013, **52**, 10426.
5 K. J. Young, L. A. Martini, R. L. Milot, R. C. Snoeberger III, V. S. Vatista, C. A. Schmuttenmaer, R. H. Crabtree and G. W. Brudvig, *Coord. Chem. Rev.*, 2012, **256**, 2503.
6 J. Sun, D. K. Zhong and D. R. Gamelin, *Energy Environ. Sci.*, 2010, **3**, 1252.
7 K. Sayama, K. Mukasa, R. Abe, Y. Abe and H. Arakawa, *Chem. Commun.*, 2001, 2416.
8 K. Fujihara, T. Ohno and M. Matsumura, *J. Chem. Soc., Faraday Trans.*, 1998, **94**, 3705.
9 C. D. Windle and R. N. Perutz, *Coord. Chem. Rev.*, 2012, **256**, 2562.
10 Y. Izumi, *Coord. Chem. Rev.*, 2013, **257**, 171.

11 A. D. Handoko, K. Li and J. Tang, *Curr. Opin. Chem. Eng.*, 2013, **2**, 200.
12 L. Alibabaei, H. Luo, R. L. House, P. G. Hoertz, R. Lopez and T. J. Meyer, *J. Mater. Chem. A*, 2013, **1**, 4133.
13 M. Morikawa, N. Ahmed, Y. Ogura and Y. Izumi, *Appl. Catal., B*, 2012, **117/118**, 317.
14 J. K. Hurst, *Science*, 2010, **328**, 315.
15 H. Gray, *Nat. Chem.*, 2009, **1**, 7.
16 N. S. Lewis and D. G. Nocera, *Proc. Natl. Acad. Sci. U. S. A.*, 2006, **103**, 15729.
17 H. Lv, Y. V. Geletii, C. Zhao, J. W. Vickers, G. Zhu, Z. Luo, J. Song, T. Lian, D. G. Musaev and C. L. Hill, *Chem. Soc. Rev.*, 2012, **41**, 7572.
18 N. Serpone, P. Maruthanuthu, P. Pichat, E. Pelizzetti and H. Hidaka, *J. Photochem. Photobiol., A*, 1995, **85**, 247.
19 F. Li and X. Duan, *Struct. Bonding*, **119**, 193.
20 K. Teramura, S. Iguchi, Y. Mizuno, T. Shishido and T. Tanaka, *Angew. Chem., Int. Ed.*, 2012, **51**, 8008.
21 M. Morikawa, N. Ahmed, Y. Yoshida and Y. Izumi, *Appl. Catal., B*, 2014, **144**, 561.
22 N. Ahmed, M. Morikawa and Y. Izumi, *Catal. Today*, 2012, **185**, 263.
23 N. Ahmed, Y. Shibata, T. Taniguchi and Y. Izumi, *J. Catal.*, 2011, **279**, 123.
24 C. Genevese, C. Ampelli, S. Parathoner and G. Centi, *J. Energy Chem.*, 2013, **22**, 202.
25 M. G. Walter, E. L. Warren, J. R. McKone, S. W. Boettcher, Q. Mi, E. A. Santori and N. S. Lewis, *Chem. Rev.*, 2010, **110**, 6446.
26 A. Kudo and Y. Miseki, *Chem. Soc. Rev.*, 2009, **38**, 253.
27 Y. Ogura and Y. Izumi, *Japanese Patent*, 2012, 223765; Y. Ogura and Y. Izumi, *Japanese Patent*, 2012, 254796; Y. Ogura, Y. Fujishima and Y. Izumi, *Japanese Patent*, 2013, 211956; Y. Ogura, S. Okamoto, T. Itoi, Y. Fujishima, Y. Yoshida and Y. Izumi, *Chem. Commun.*, 2014, **50**, 3067.
28 R. Yadav and P. S. Fedkiw, *J. Electrochem. Soc.*, 2012, **159**, B340.
29 F. Quentel, G. Passard and F. Gloaguen, *Chem. - Eur. J.*, 2012, **18**, 13473.
30 S. Kaneco, H. Kurimoto, Y. Shimizu, K. Ohta and T. Mizuno, *Energy*, 1999, **24**, 21.
31 N. M. Dimitrijevic, B. K. Vijayan, O. G. Poluektov, T. Rajh, K. A. Gray, H. He and P. Zapal, *J. Am. Chem. Soc.*, 2011, **133**, 3964.
32 N. Zhang, S. Ouyang, T. Kako and J. Ye, *Chem. Commun.*, 2012, **48**, 1269.
33 S. N. Habisreutinger, L. Schmidt-Mende and J. K. Stolarczyk, *Angew. Chem., Int. Ed.*, 2013, **52**, 7372.
34 Y. Yoshida, Y. Mitani, T. Itoi and Y. Izumi, *J. Catal.*, 2012, **287**, 190.
35 C. Wang, R. L. Thompson, J. Baltrus and C. Matranga, *J. Phys. Chem. Lett.*, 2010, **1**, 48.
36 Y. T. Liang, B. K. Vijauyan, K. A. Gray and M. C. Hersam, *Nano Lett.*, 2011, **11**, 2865.